Improving zinc porous electrode for secondary alkaline batteries: Toward a simple design of optimized 3D conductive network current collector

Vincent Caldeira, Julien Thiel, François René Lacoste, Laetitia Dubau, Marian Chatenet

Version of Record: https://www.sciencedirect.com/science/article/pii/S0378775319316611
Manuscript_854b398f2f626cb202b36ac90cd390a4

Improving Zinc Porous Electrode for Secondary Alkaline Batteries: Toward a Simple Design of Optimized 3D Conductive Network Current Collector

Vincent Caldeira[a,b], Julien Thiel[b], François René Lacoste[b], Laetitia Dubau[a], Marian Chatenet[a]

[a] Univ. Grenoble Alpes, Univ. Savoie Mont Blanc, CNRS, Grenoble INP (Institute of Engineering Univ. Grenoble Alpes), LEPMI, 38000 Grenoble, France

[b] EASYL SA, 712 Avenue de Faucigny, 74130 Bonneville, France

Abstract

The internal migration of zinc within the thickness of porous composite negative electrodes for rechargeable zinc batteries causes detrimental shape change of the zinc electrode. It depends on various parameters linked to the electron conduction in the electrode: electronic percolation, conductive additives, primary current collector. This study highlights a simple solution, that drastically improves the electrochemical performance of thick and porous zinc electrodes, by rethinking their architecture. Using a multiplicity of thin current collectors enables to create a 3D network of electronic percolation and a better repartition of the current lines within the electrode; as a result, the formation of multiple active zinc cores in the electrode volume is better controlled. This strategy allows to better manage zinc migration within the electrode structure, leading to minimal densification of each zinc core, and overall enables higher reversibility of zinc oxidation/reduction upon discharge/charge. It finally mitigates the initial drastic capacity fading observed on standard type calcium zincate negative electrode.

Graphical Abstract

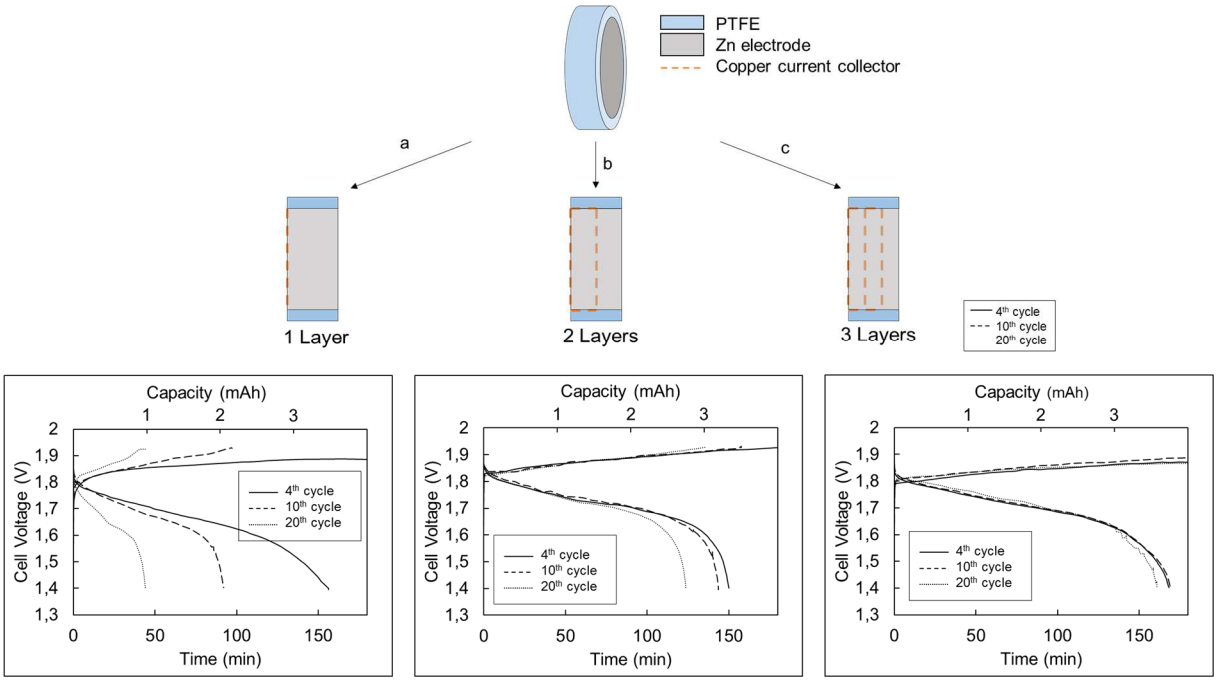

Keywords

Zinc-Nickel (Zn / Ni) batteries, Multilayer current collector, Migration control, Core-shell mechanism

1. Introduction

Global warming, pollution, energy consumption, non-renewable sources, fossil fuels... These words are overwhelming the international scientific community and are levers that enable to improve scientific and technological aspects of “green” energy. In response, dedicated works concern electrochemical storage and conversion systems, which are widely used and developed for automotive and stationary applications. Among a wide portfolio of batteries, alkaline ones with zinc negative electrodes, either zinc-air or zinc-nickel systems, are interesting candidates, owing to their attractive specific capacity, high power density, safety and environmental friendliness [1]. They are essentially composed of abundant and non-toxic materials and can be manufactured through environmental-friendly processes. However, these technologies have lost attention in the 1980s, because of the emergence of more energetic Li-ion batteries. Zinc batteries usually suffer from non-negligible capacity loss and low cycle life, caused by multiple phenomena that occur during their charge and discharge. For example, shape change of the zinc electrode, a phenomenon caused by a heterogeneous migration of zinc within the electrode, leads to drastic morphological changes and contributes to long-term cycle life failure. Many research works have aimed to mitigate shape change, notably by using additives in the electrodes [2–7]. Usually, zinc electrodes are made of a blend of zinc oxide with conductive additives, shape change stabilizer, fibrous polymer binder, etc. in an aqueous media, pasted onto the current collector, before being dried and rolled/laminated/pressed. In most studies, a single layer of current collector is used per zinc negative electrode, either as porous (foam [8–10], expanded/mesh/gauze/ribbon metal [11,12,21,22,13–20]) or as foil/sheet [23–26] structures. Recently, copper foams emerged as the most employed primary current collector materials.

The literature usually suggests that zinc electrode shape change is a surface modification phenomenon, but a novel mechanism has been recently proposed for thick porous electrodes [27]: the migration of zinc responsible for the shape change would occurs within the core of the electrode, in the vicinity of the primary current collector, leading to the formation of a partially-active zinc core. This internal phenomenon follows a working gradient within the thickness of the electrode, coming from the current

collector to the surface of the electrode. In a desired configuration, the current collector is not in direct contact with the electrolyte to avoid dendrite formation. As thick zinc electrodes are not used at 100% of their theoretical capacity, but instead with a nominal capacity selected between a few 10% and 80% of the theoretical capacity, the surface of the electrode remains intact, after repeated charge/discharge cycles, which shall reduce the possibility of dendrite formation and maintain the active part of the electrode within the core. However, this new mechanism is accompanied by its own problem, which is the self-densification of the zinc core. During repetitive cycling, as the zinc core is only partially active, because of the local inaccessibility of zinc resulting from porosity plugging, and as the demand in energy is the same for each charge/discharge cycle, zinc must increasingly be utilized towards the electrode surface (further away from the primary current collector from cycle to cycle). This densification likely reduces the mass and charge transfer kinetics, at least in the vicinity of this zinc core, inducing cell overvoltage and practical capacity loss.

In order to prevent those eventual drawbacks, electrodes embedding a multiplicity of primary current collector were designed and patented [28]. This study shows the potential of the invention and reports how controlling the formation of a multitude of small zinc cores (on each multilayered current collector), instead of a large one as usually observed in model (thick) zinc-based electrodes, improves the electrochemical performances. Such laboratory-scaled electrodes were prepared and cycled using a homemade designed Swagelok cell, and analyzed *post*-test using cross-section scanning electron microscopy, to follow the fate (possible redistribution) of zinc and of the electrode additives within the composite electrode.

2. Experimental

2.1. Preparation of Zn electrodes for 10 mAh theoretical laboratory Swagelok cell

Circular calcium zincate-based mono-facial electrodes were prepared by deposition of an aqueous ink on one layer of a copper current collector (Fig. 1). The ink was composed of calcium zincate synthesized by a hydro-micromechanical (EASYL supplier d_{50} = 10 ± 2 µm) [29,30] as active material, titanium nitride and bismuth oxide as conductive additives, and polyvinyl alcohol (Fluka 72 000 Mw) as binder, in which the corresponding mass ratio was 73:12:5:10. Depending on the number of current collectors used (1, 2 or 3), the amount of electrode material deposit was adapted: 1 layer = 30 mg, 2 layers = 2 × 15 mg and 3 layers = 3 × 10 mg of calcium zincate equivalent active material mass. The number of layers was defined by the amount of copper and the practical limit of processing, because of thinner layers of electrode matter, that affects the adhesion and robustness of the layers (at least using this ink process). After drying the deposit in an oven at T = 50°C, the layers were superposed, placed inside a PTFE ring and pressed (1.5 T). The PTFE ring aim to protect the edge of the electrodes, avoiding dendrite formation on the sides, and allowing to have the same electrode/electrolyte surface. A copper foam, 300 g/m², was used as model electrode for the "1 layer" electrode and copper mesh (100 g/m², with wire diameter = 70 µm) was used as multilayer current collector. The choice of these current collector is based on their economic and ecologic value: the manufacturing process to obtain copper foam needs heavy chemical processing, hence high economic and ecological price compared to copper grids. Pasted NiOOH/$Ni(OH)_2$ on nickel foam was used as counter-electrode with an over-dimensioned capacity, to perform this study with the zinc electrode as the limiting electrode. The NiOOH/$Ni(OH)_2$ electrodes were extracted from a commercial ZnNi cell. The working and counter electrodes were separated with a nonwoven polyolefin separator (Viledon®) and a polypropylene membrane (Celgard®), assembled in a homemade designed cell, made from a PFA T-type tubing pipe from Swagelok®, and filled with an aqueous solution of 7 M KOH with 10 g/L LiOH [4] and saturated in ZnO as electrolyte. In the present configuration of electrode, the current collector is not directly exposed to the electrolyte (it is considered as the core of the electrode); the surface of the electrode, considered as the shell, was directly exposed to the electrolyte and faces the separator soaked with electrolyte and then the counter electrode; the cell geometry is detailed in supplementary information Fig.Si. 1. The nominal capacity was based on 40% of the theoretical capacity, thus used between 40% of SOC and 100% of DOD. A potentiostat-galvanostat OGF500

(Origalys, France) was used to perform galvanostatic cycling at C / 3 with U_{cutoff} = 1.93 V (at room temperature) to avoid adverse overvoltage and hydrogen formation. Before cycling, electrode formation was applied following 3 cycles at C / 10 in charge and C / 5 in discharge.

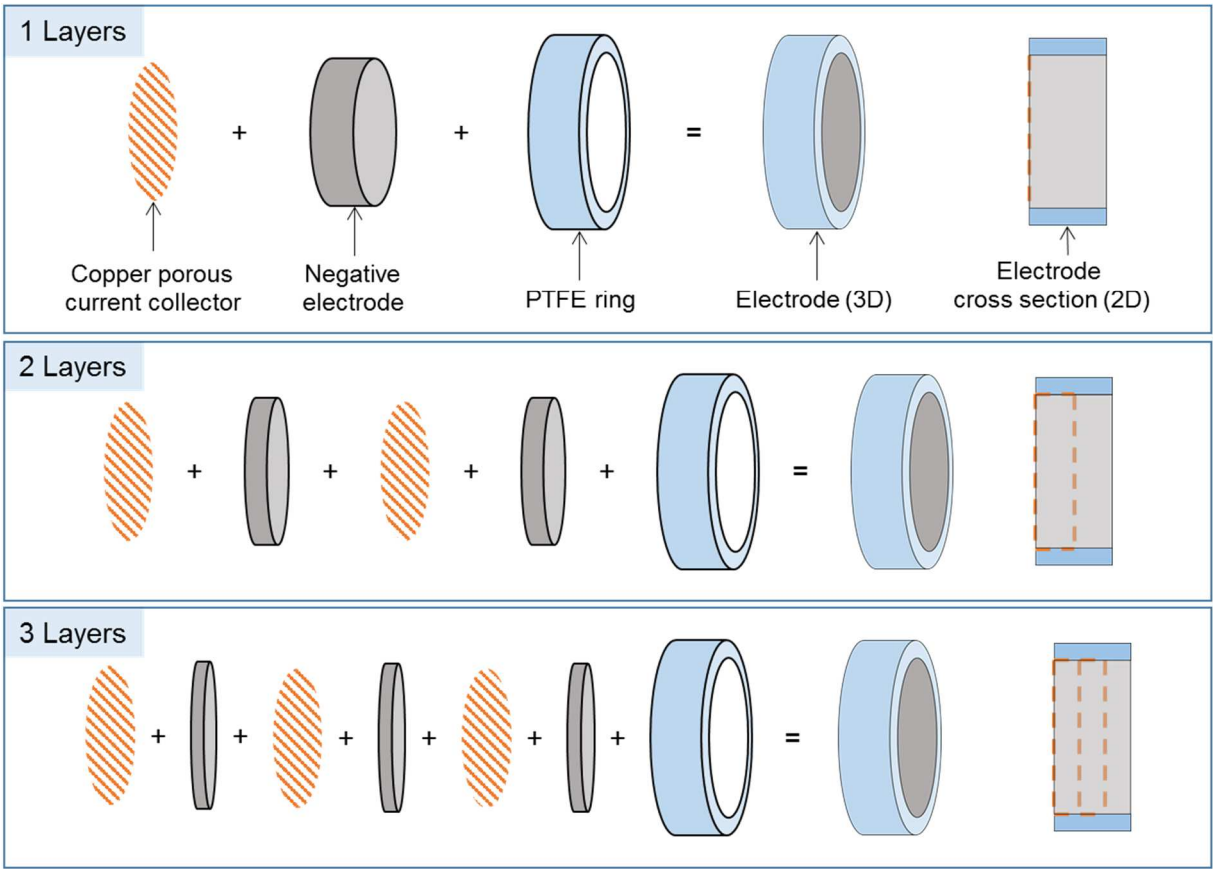

Fig. 1. Schematic representation of zinc-based electrodes with 1 layer copper foam (a), 2 layers of copper mesh (b) and 3 layers of copper mesh (c)

2.2. Physico-chemical characterizations

Post-test analyses were used to characterize the new/aged composite electrodes. These essentially consist of electron microscopy imaging on electrode cross-sections. To that goal, the electrodes were embedded inside an epoxy resin and polished until mid-height with a mirror-finish. A carbon coating was applied on the resin-embedded samples, using a carbon evaporator (BALTEC CED030, Bal-Tec Union Ltd., Liechtenstein), to avoid any surface charge effect under the electron beam. Morphological

analyses were achieved using a field-emission gun scanning electron microscope (FEG-SEM Ultra 55, Carl Zeiss, Germany) working at U_{HT} = 20 KeV as acceleration voltage within a minimum time laps after sample preparation to prevent surface modification or atmospheric corrosion. Back-Scattered electron imaging (BSD) and X-ray Energy dispersive spectroscopy mapping (X-EDS) were performed to provide colored elemental maps (each color being linked to an element) to visualize the elemental distribution within the electrode thickness. The color convention used in this paper was: zinc in red, calcium in green, titanium in dark blue and copper in bright blue. As bismuth oxide was present in small amounts in the electrode and in order to minimize the numbers of colors on the micrographs (for clarity), this element was not affiliated to any color (and appears white in the chemical maps).

3. Results and Discussions

3.1. Internal morphological evolution of calcium zincate-based electrodes and prediction

Our previous work [27] revealed a mechanism of the formation of a zinc core in porous bifacial zinc-based electrodes, made either with calcium zincate or a mix of zinc oxide and calcium hydroxide. The apparition of agglomerated zinc oxide in the vicinity of the copper foam upon the ageing of the electrode is driven by a working gradient, as observed using laboratory-scale mono-facial electrodes. Herein, investigations were oriented towards newly designed monofacial electrodes (see Fig. 1). Fig. 2. compiles multiple FEG-SEM micrographs taken along negatives electrodes after only one formation cycle (a) and after 50 charge/discharge cycles (b); 5 micrographs per electrodes were assembled to show the full electrodes in cross-section. The specific methodology to obtain this result is detailed in supplementary information (Fig.Si. 2).

The delimited area in dashed red line represents the morphologically-modified material. After the formation cycle (Fig. 2.a.), zinc clusters are present close to the copper foam (bright blue) and around

agglomerated titanium (dark blue), which confirms zinc preferential migration towards highly-electron-conductive zones. Using ImageJ software, area measurement shows that ca. 36% of the equivalent total surface of the electrode thickness was used, value in agreement with the nominal capacity (C_N = 40% of the theoretical capacity); this suggests that the volume of used active material initially corresponds to the chosen nominal capacity. In the present case, one notes that the working thickness repartition is heterogeneous and more important in the middle: a higher concentration of zinc (red) is observed in the middle.

After 50 charge/discharge cycles at C/3 (Fig. 2.b.), zinc cluster are displaced and electrodeposited onto the copper foam (red clusters on the bottom of the micrograph), creating zinc-depleted volumes along the electrode and consequently rich calcium regions (green). The surface of the electrode is still composed of the pristine calcium zincate material and additives, thereby confirming the core-shell mechanism. Zinc densification on itself upon cycling reduces its active surface area, and, as the charged capacity was kept constant, this leads to a necessary reduction of ZnO/zincate towards the outer volume of the electrode (further from the Cu-foam current collector) upon charge. Using the same technique of morphologically-modified volume determination by ImageJ on Fig. 2.b., one calculates that 65% of the whole electrode volume has been used at that stage.

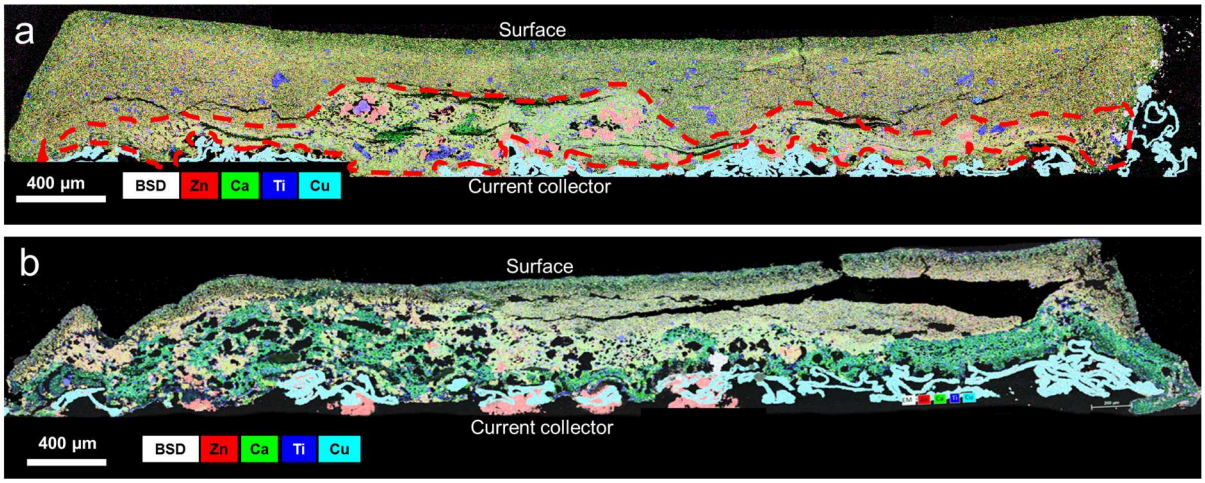

Fig. 2 Compilation of multiple FEG-SEM X-EDS elemental mapping micrographs representative of a complete model negative electrode in cross-section, after a formation cycle (a) and after 50 cycles at C/3 (b). The red dashed line delimits the morphologically modified zones.

To prevent this gradual increase of the volume of used material, a simple and industrially scalable solution is proposed. If zinc clusters appear upon charge (which initiates in the formation cycles), the volume of used material must be controlled to prevent major segregation. From this statement, the idea of using more than one (primary) current collector appears obvious. In order to not increase the weight of copper current collector per electrode (300 g/m² for a Cu-foam collector), it has been chosen to use two or three layers of lighter copper grid (100 g/m²).

Fig. 3**.** is a schematic representation of the volume of active electrode during repeated charge/discharge cycling in conventional electrodes compared to the layered architecture. In this simple representation, the volume of active electrode is denoted by V_1 and the inactive one by V_2. *Eq1* represents the volume total of electrode (V_3):

$$V_3 = V_1 + V_2 \qquad \textit{Eq.1.}$$

If the correlation between the active volume obtained from cross-section microscopy and the nominal used capacity, noted C_N above, the working volume in such electrode could be predicted using:

$$V_1 = C_N \text{ x } V_3 \qquad \textit{Eq.2.}$$

Introducing the idea of multiplying the number "*n*" of current collector within the thickness of the electrode, it could be possible to predict the active volume surrounded each layer of current collector "V_n" using *Eq.3.*

$$V_n = V_1 / n \qquad \textit{Eq.3.}$$

This simple idea, using basic elementary grade scholar equations, represents for the example in Fig. 3, 1 x 40% of active volume in model electrode (a) *versus* 13.3% per current collector in the three-layered electrode (b), for the same nominal capacity C_N = 40%. Besides, electrodes made using this

process are open to customization (number of layers, thickness, composition…). As a proof of concept, Fig. 3.c. represents an example of "*n* = 3" layered conductive network calcium zincate electrode after 3 cycles of formation. X-EDS elemental mapping confirms the presence of active zones "A" constituted by a sponge-mix including active calcium zincate, zinc oxide and calcium hydroxide and alternatively superposed to inactive zones "B" constituted by lamellar calcium zincate. This last composed the surface of the electrode, named "shell" in this technology.

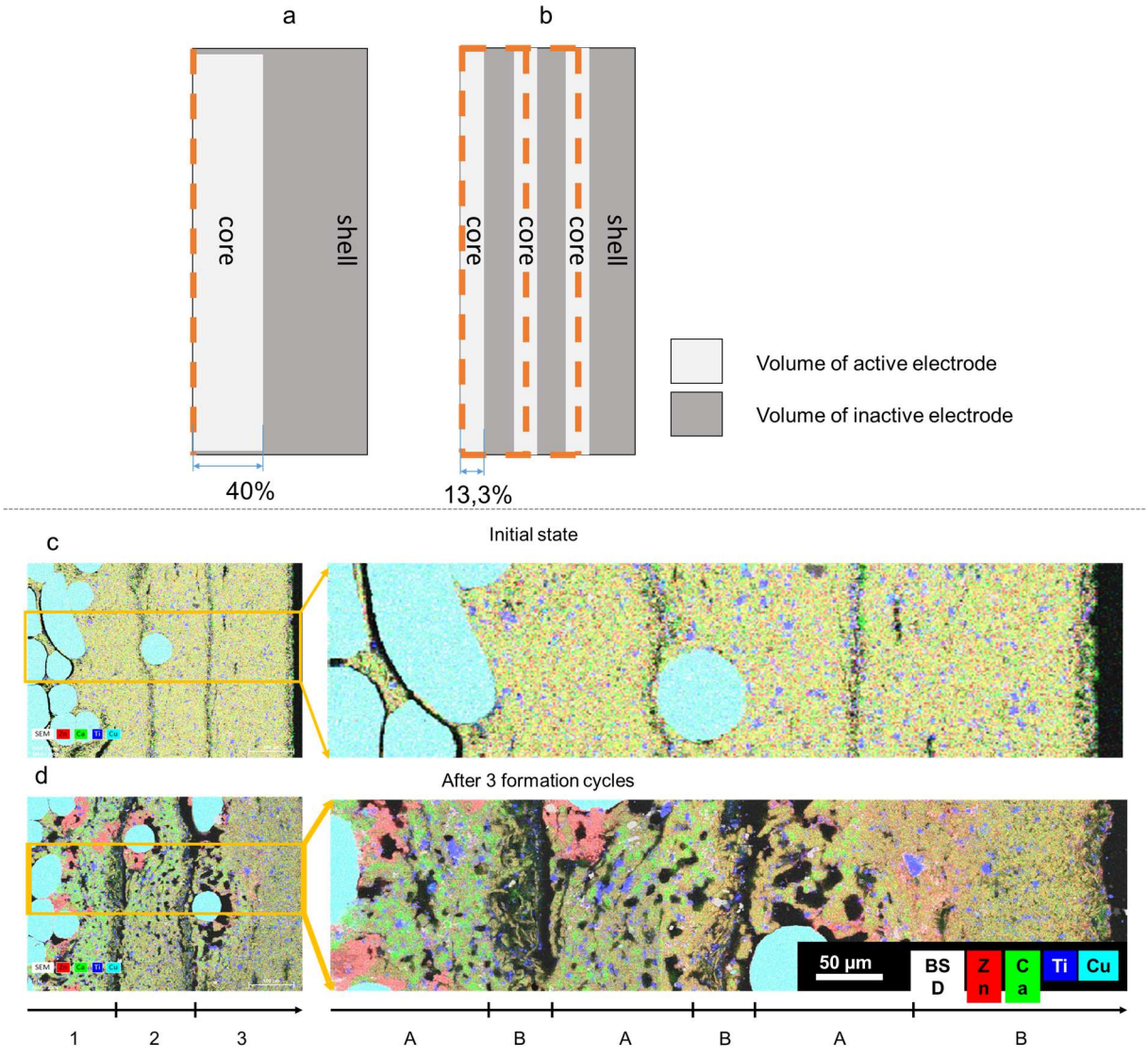

Fig. 3. Schematic representation of active core during cycling in model (a) versus "n = 3" layered conductive network porous zinc-based electrode (b) and FEG-SEM X-EDS elemental mapping of a "n = 3" layered conductive network calcium zincate based electrode in cross-section at initial state (c) and after 3 cycles of formation at C/10 (d).

3.2. Electrochemical and morphological investigation of calcium zincate-based electrode with "*n*" layers of current collector

In the aim to investigate the electrochemical performances stability of electrodes with $1 \leq n \leq 3$, circular calcium zincate-based mono-facial electrodes of 10 mAh theoretical capacity were elaborated and cycled 50 times in charge / discharge at 4 mAh of nominal capacity (C_N = 40% of 10 mAh). Fig. 4**.** presents morphological and electrochemical performances of model electrodes with "*n* = 1", "*n* = 2" and "*n* = 3" layer of copper current collector. In agreement with our previous work [27], cross-section X-EDS mapping shows the core-shell mechanism of operation of the porous electrode: zinc migration is observed in the vicinity of the copper foam (primary current collector). Electrodes in this study are made with calcium zincate as active material (discharge state), which means that zinc is chemically linked to calcium, at least initially (before the first charge). The zinc migration observed necessary means that calcium and zinc segregation from initial zincate has occurred, leading to the formation of a calcium-rich layer located between each zinc-core and still unused calcium zincate regions. Calcium hydroxide being electro-inactive and electronic-insulant, the formation of a separate layer between the zinc core and active calcium zincate means a loss of electrical contact, and only the core of zinc can be easily reached to perform the electrochemical oxidation-reduction reactions. This phenomenon is responsible for additional overvoltage contributions starting at cycle 10 below 100 min of charging, that reach the cut-off voltage of 1.93 V, and below 50 min at the 20th charge, yielding a drastic decrease of the practical capacity. The output average median voltage was 1.66 V. The calculated average capacity of this electrode for the first 50 cycles is 1.27 mAh, which means that only 32% of the initial nominal capacity has been retained.

In order to reduce/avoid this phenomenon, by reducing the ohmic resistance, electrodes with "*n* > 1" layers of (primary) current collector were elaborated with the same formulation; they were charged and discharged 50 times and *post*-tested. The electrode with "*n* = 2" shows less pronounced overvoltage for cycle 10 and 20 during the charge and an output average median voltage equivalent to 1.72 V, but zinc segregation is still observed in X-EDS mapping. Even if zinc migration cannot be

completely avoided, it is at least enough reduced to prevent the formation of a detrimentally-large and continuous layer of resistive calcium hydroxide, which is believed to be responsible for the appearance of the cell overvoltage. For the electrode with "n = 2", the average capacity is 2.3 mAh for the first 50 cycles, corresponding to 58% of nominal capacity retention.

Finally, the "n = 3" layered calcium zincate-based electrode confirms the predicted behavior: zinc-calcium segregation leads to the formation of multiple small zinc clusters (in red) always close to the individual copper grids (bright blue) and surrounded by calcium-rich areas (green). The surface of the electrode, at the right of the image, presents initial calcium zincate crystals (yellow), that have not been used and still protect the electrode surface from dendrite growth. As expected from section 2.1., the active material seems efficiently used along the thickness of the electrode and with gradual performances related to "n" (the performances evolve as follows: "n = 3" > "n = 2" > "n = 1"). As a result, the "n = 3" calcium zincate-based electrodes show an average nominal capacity retention of 92% after 50 cycles and 1.71 V as output average median voltage. So not only the multiple current collectors enable larger capacity retention after 50 charge/discharge cycles, but also larger median voltage, hence practical larger energy. Note that for all the cases, the outer surface of electrodes remains unused – it is considered as a shell – and thus protects the core of the electrode from any dendrite growth.

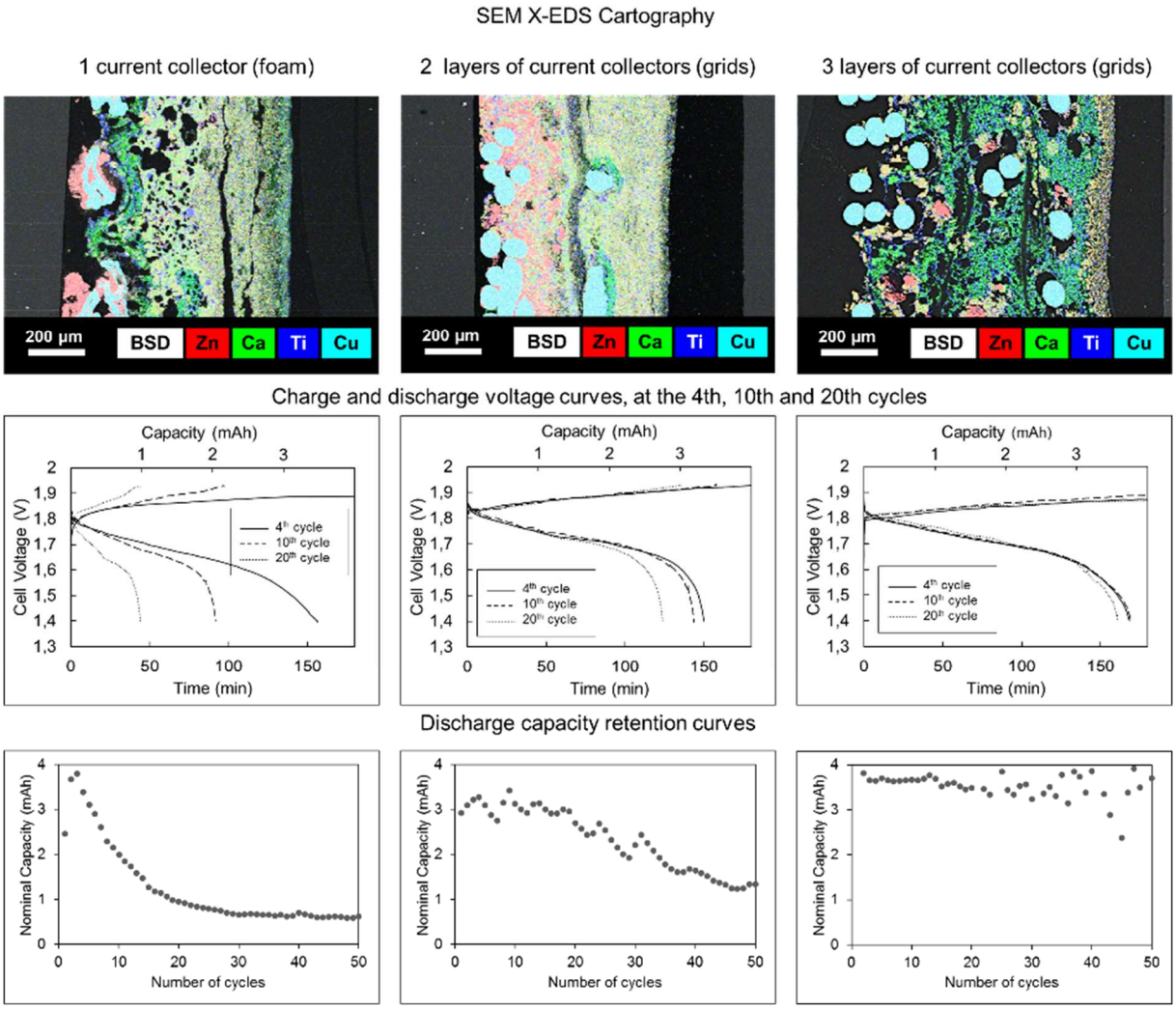

Fig. 4. FEG-SEM X-EDS elemental mapping of cross-sectioned electrodes, charge and discharge voltage curves and capacity retention curves of electrodes composed with 1 copper foam current collector compared to "n = 2" and "n = 3" layered copper current collector.

4. Conclusion

As zinc-based electrode technology seems to be at a standstill of technological development, a new look has been made on how its current collection could be improved. This study highlights a simple and industrially-scalable way to improve thick zinc-porous electrodes by using an optimized conductive network of layered primary current collector. By reducing zinc segregation along the thickness of the electrodes, the multiple layers of current collector lead to improved electrochemical performances of calcium zincate-based electrodes and overcome the initial drastic capacity fading

observed on standard configuration. This study shows the potential of such strategy at small electrode scale and opens the gate to prototype studies in order to confirm the enhancement in electrochemical performances for larger electrodes. Moreover, this invention could be easily applied to well-defined and mature manufacturing bases to create ultra-thick electrodes for high capacity systems such as Zinc-Air stationary application.

Acknowledgments

The author would like to thanks La Fondation de France (Grant n°0049328) and CNRS (Grant n°113815) for the financial support.

Conflict of interest

The authors declare no conflict of interest regarding the publication of this paper.

References

[1] D. Linden, T.B. Reddy, Handbook of Batteries, third edition, 2002. doi:10.1016/0378-7753(86)80059-3.

[2] J. McBreen, E. Gannon, The electrochemistry of metal oxide additives in pasted zinc electrodes, Electrochim. Acta. 26 (1981) 1439–1446. doi:10.1016/0013-4686(81)90015-3.

[3] J. McBreen, E. Gannon, Bismuth oxide as an additive in pasted zinc electrodes, J. Power Sources. 15 (1985) 169–177.

[4] K. Bass, P.J. Mitchell, G.D. Wilcox, J. Smith, Methods for the reduction of shape change and dendritic growth in zinc-based secondary cells, J. Power Sources. 35 (1991) 333–351. doi:10.1016/0378-7753(91)80117-G.

[5] F.R. McLarnon, The Secondary Alkaline Zinc Electrode, J. Electrochem. Soc. 138 (2006) 645. doi:10.1149/1.2085653.

[6] Y. Zheng, J.M. Wang, H. Chen, J.Q. Zhang, C.N. Cao, Effects of barium on the performance of secondary alkaline zinc electrode, Mater. Chem. Phys. 84 (2004) 99–106. doi:10.1016/j.matchemphys.2003.11.015.

[7] J. Cheng, Z. Zhang, Y. Zhao, W. Yu, H. Hou, Effects of additives on performance of zinc electrode, Trans. Nonferrous Met. Soc. China. 24 (2014) 3551–3555. doi:10.1016/S1003-6326(14)63500-7.

[8] E.C. Gay, F.J. Martino, Method for preparing electrode with porous current collector structures and solid reactants for secondary electrochemical cells, United States Pat. (1976).

[9] Y.F. Yuan, L.Q. Yu, H.M. Wu, J.L. Yang, Y.B. Chen, S.Y. Guo, J.P. Tu, Electrochemical performances of Bi based compound film-coated ZnO as anodic materials of Ni-Zn secondary batteries, Electrochim. Acta. 56 (2011) 4378–4383. doi:10.1016/j.electacta.2011.01.006.

[10] F. Moser, F. Fourgeot, R. Rouget, O. Crosnier, T. Brousse, In situ X-ray diffraction investigation of zinc based

electrode in Ni–Zn secondary batteries, Electrochim. Acta. 109 (2013) 110–116. doi:10.1016/j.electacta.2013.07.023.

[11] R. Jain, T.C. Adler, F.R. McLarnon, E.J. Cairns, Development of long-lived high-performance zinc-calcium/nickel oxide cells, J. Appl. Electrochem. 22 (1992) 1039–1048. doi:10.1007/BF01029582.

[12] M. Rivers, L.A. Tinker, Multi-layer current collector, United States Pat. (1999).

[13] N.A. Hampson, A.J.S. McNeil, The Electrochemistry of Porous Zinc V. The cycling behaviour of plain and polymer-bonded porous electrodes in KOH solutions, J. Power Sources. (1985).

[14] W. Gan, D. Zhou, L. Zhou, Z. Zhang, J. Zhao, Zinc electrode with anion conducting polyvinyl alcohol/poly(diallyldimethylammonium chloride) film coated ZnO for secondary zinc air batteries, Electrochim. Acta. 182 (2015) 430–436. doi:10.1016/j.electacta.2015.09.105.

[15] Y. Wen, T. Wang, J. Cheng, J. Pan, G. Cao, Y. Yang, Lead ion and tetrabutylammonium bromide as inhibitors of the growth of spongy zinc in single flow zinc/nickel batteries, Electrochim. Acta. 59 (2012) 64–68. doi:10.1016/j.electacta.2011.10.042.

[16] J. Jindra, Sealed nickel-zinc cells, J. Power Sources. 37 (1992) 297–313. doi:10.1016/0378-7753(92)85014-2.

[17] J.T. Nichols, F.R. McLarnon, E.J. Cairns, Active material redistribution rates in zinc electrodes: effect of alkaline electrolyte compositions having reduced zinc oxide solubility, M.S. Thesis. 139 (1984) 79–96. doi:10.1149/1.2221597.

[18] G. Li, K. Zhang, M.A. Mezaal, R. Zhang, L. Lei, Effect of electrolyte concentration and depth of discharge for zinc-air fuel cell, Int. J. Electrochem. Sci. 10 (2015) 6672–6683.

[19] K. Wang, P. Pei, Z. Ma, H. Xu, P. Li, X. Wang, Morphology control of zinc regeneration for zinc–air fuel cell and battery, J. Power Sources. 271 (2014) 65–75. doi:10.1016/j.jpowsour.2014.07.182.

[20] R.G. Gunther, R.M. Bendert, Zinc Electrode Shape Change in Cells with Controlled Current Distribution NiOOH NiOOH, J. Electrochem. Soc. (1987) 782–791. doi:10.1149/1.2100573.

[21] R. Othman, A.H. Yahaya, A.K. Arof, Zinc-Air Cell with KOH-Treated Agar Layer between Electrode and Electrolyte Containing Hydroponics Gel, J. New Mater. Electrochem. Syst. 5 (2002) 177–182.

[22] A. Striebel, Laboratory-scale evaluation of secondary batteries for electric vehicles, J. Power Sources. 47 (1994) 1–11.

[23] S. Muller, F. Holzer, O. Haas, Optimized zinc electrode for the rechargeable zinc ± air battery, J. Appl. Electrochem. 28 (1998) 895–898.

[24] J. PHILLIPS, High rate, thin film, bipolar, nickel zinc battery having oxygen recombination facility, Can. Intellect. Prop. Off. (2003).

[25] L. Zhong, X. Xi, Electrode formation by lamination of particles onto a current collector, 2005. doi:US 2010/0311130 Al.

[26] D.E. Turney, M. Shmukler, K. Galloway, M. Klein, Y. Ito, T. Sholklapper, J.W. Gallaway, M. Nyce, S. Banerjee, Development and testing of an economic grid-scale flow-assisted zinc/nickel-hydroxide alkaline battery, J. Power Sources. 264 (2014) 49–58. doi:10.1016/j.jpowsour.2014.04.067.

[27] V. Caldeira, R. Rouget, F. Fourgeot, J. Thiel, F. Lacoste, L. Dubau, M. Chatenet, Controlling the shape change and dendritic growth in Zn negative electrodes for application in Zn/Ni batteries, J. Power Sources. 350 (2017) 109–116. doi:10.1016/j.jpowsour.2017.03.069.

[28] V. Caldeira, L. Dubau, M. Chatenet, Electrode with current collection multiple array, Int. Pat. WO 2019/04 (2019).

[29] F.R. Lacoste, J. Thiel, Method for manufacturing calcium zincate crystals, and the uses thereof, French Pat. (2016).

[30] V. Caldeira, L. Jouffret, J. Thiel, F.R. Lacoste, S. Obbade, L. Dubau, M. Chatenet, Ultrafast Hydro-Micromechanical Synthesis of Calcium Zincate: Structural and Morphological Characterizations, J. Nanomater. 2017 (2017) 1–8. doi:10.1155/2017/7369397.

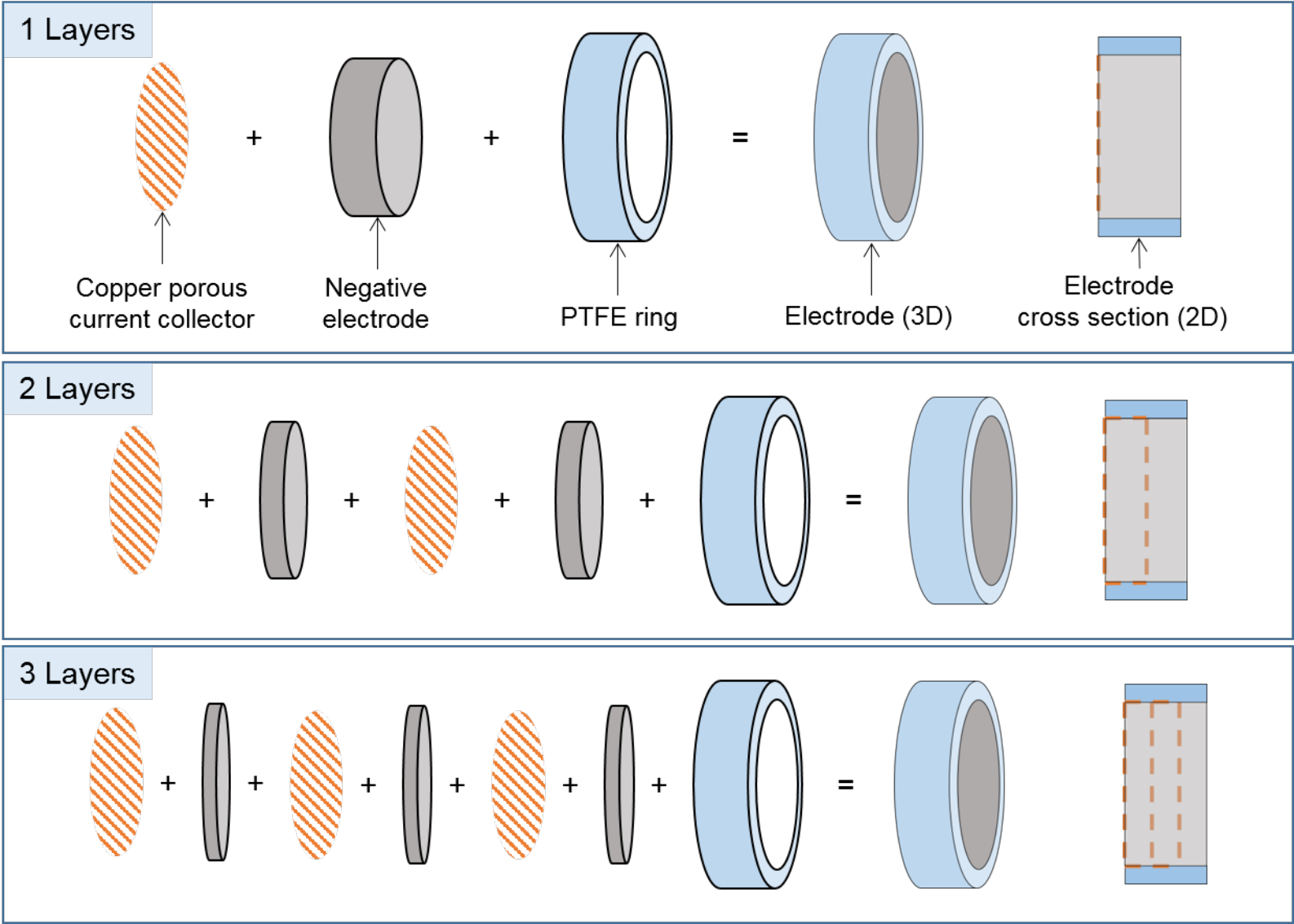
1 Layers
+
+
=
Copper porous current collector
Negative electrode
PTFE ring
Electrode (3D)
Electrode cross section (2D)
2 Layers
+
+
+
+
=
3 Layers
+
+
+
+
+
+
=

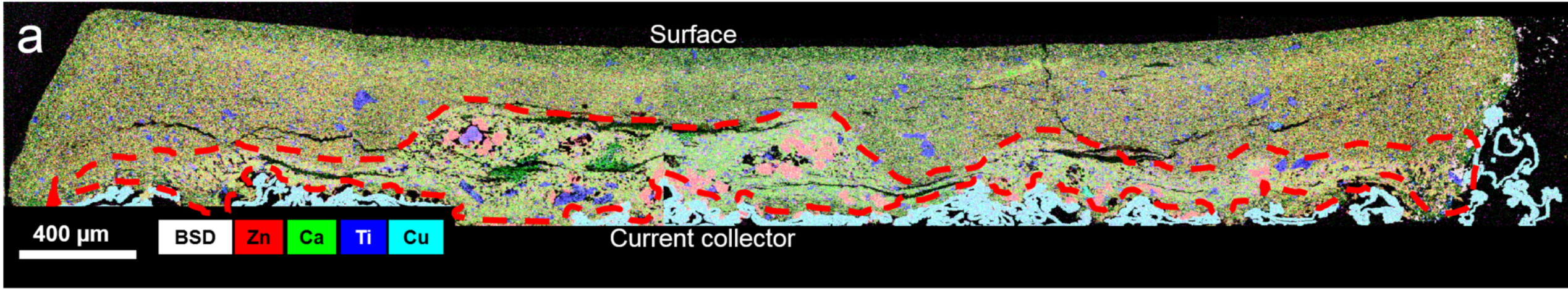
a
Surface
400 μm
BSD
Zn
Ca
Ti
Cu
Current collector

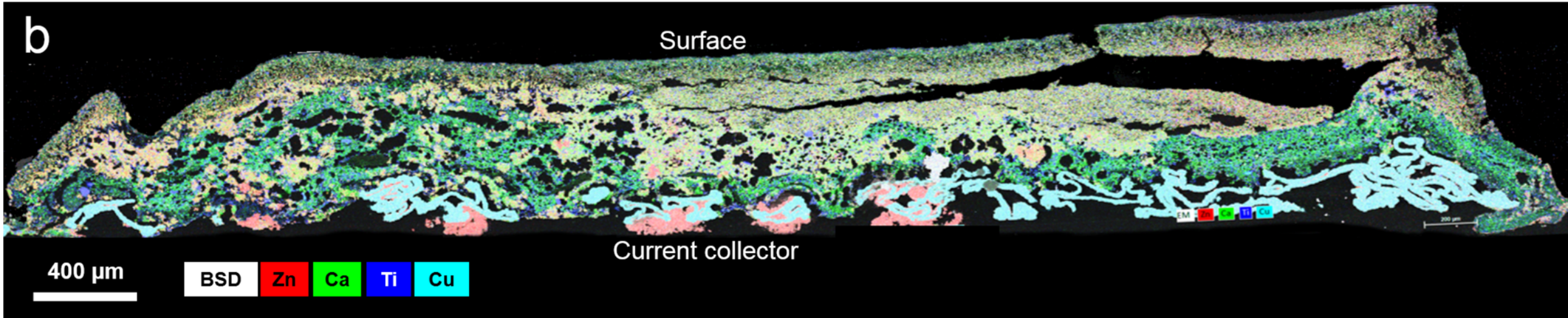
b
Surface
400 μm
BSD
Zn
Ca
Ti
Cu
Current collector

a

b

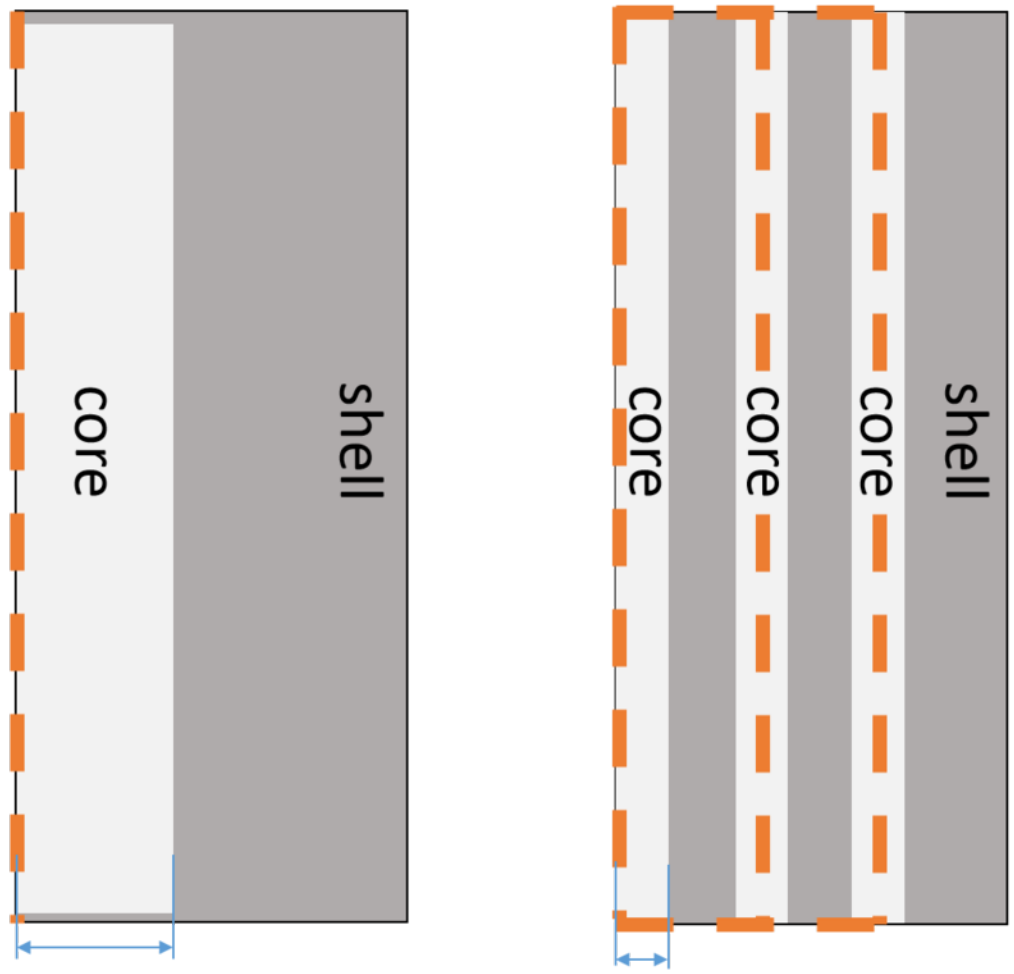

c

Initial state

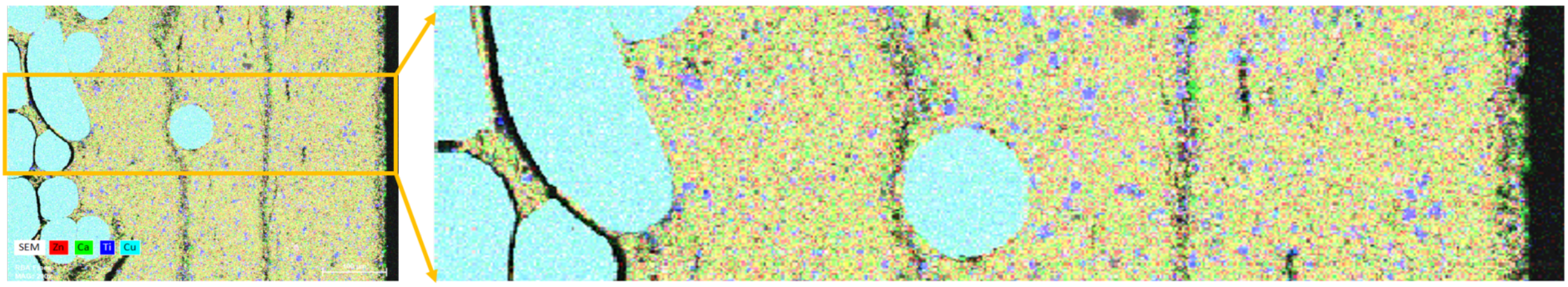

d

After 3 formation cycles

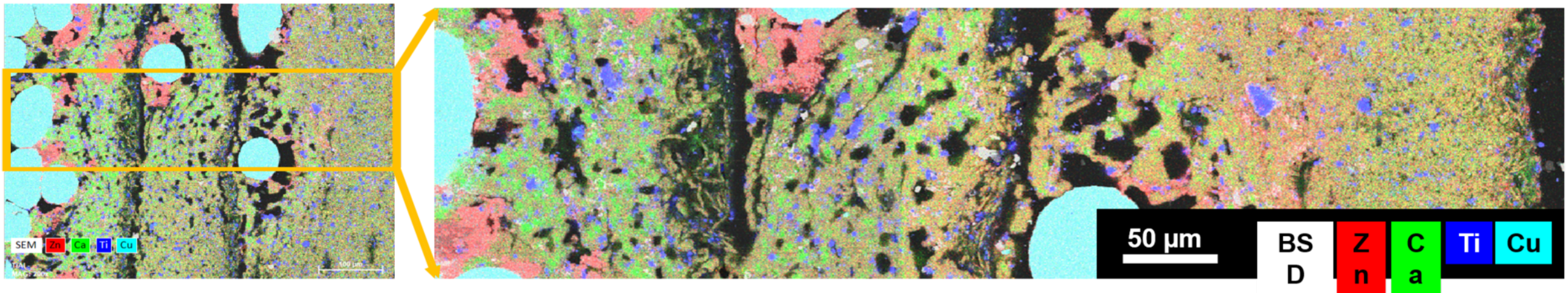

1 2 3 A B A B A B

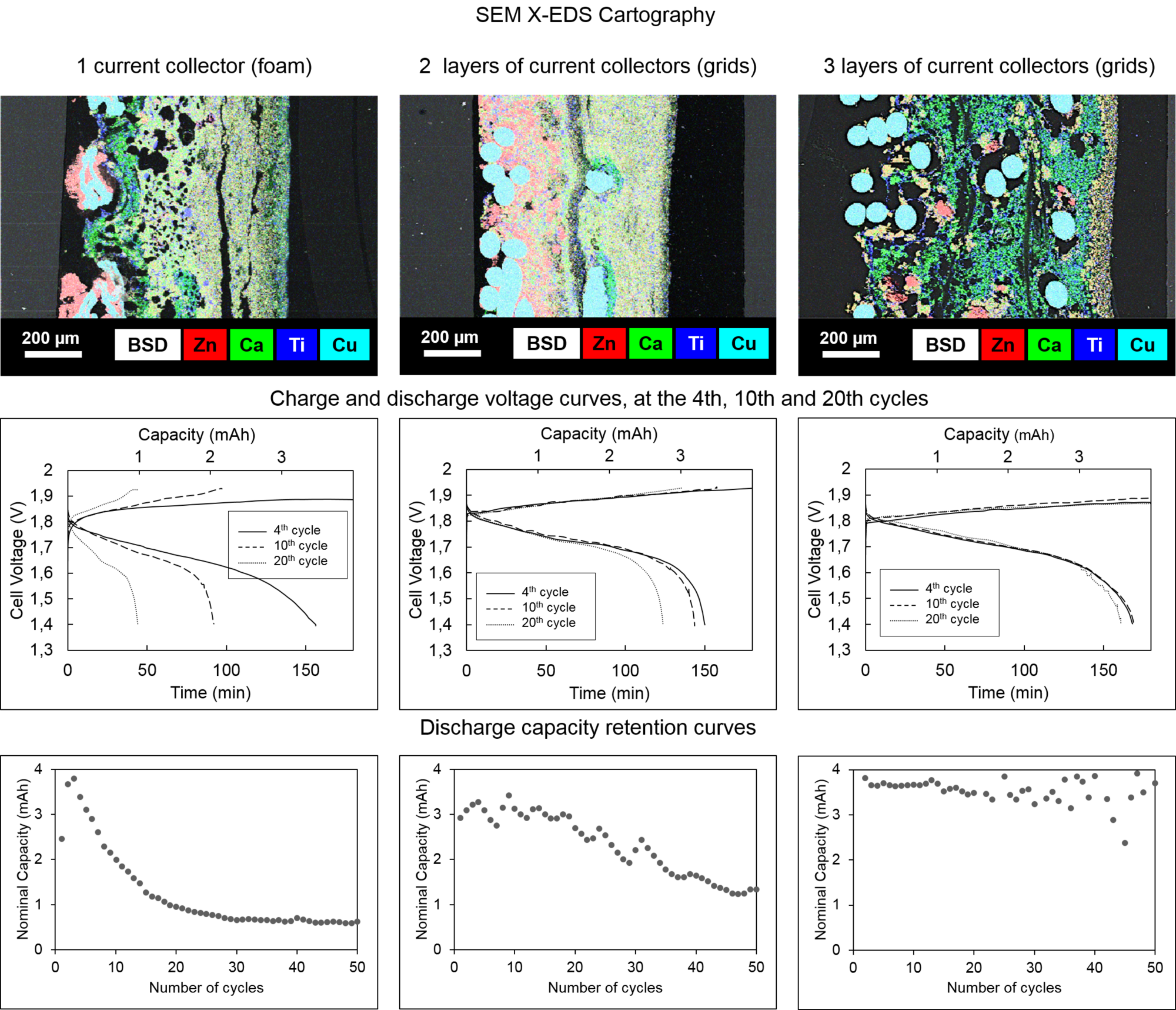

SEM X-EDS Cartography
1 current collector (foam)
2 layers of current collectors (grids)
3 layers of current collectors (grids)
200 µm
BSD
Zn
Ca
Ti
Cu
Charge and discharge voltage curves, at the 4th, 10th and 20th cycles
Capacity (mAh)
Cell Voltage (V)
Time (min)
4th cycle
10th cycle
20th cycle
Discharge capacity retention curves
Nominal Capacity (mAh)
Number of cycles

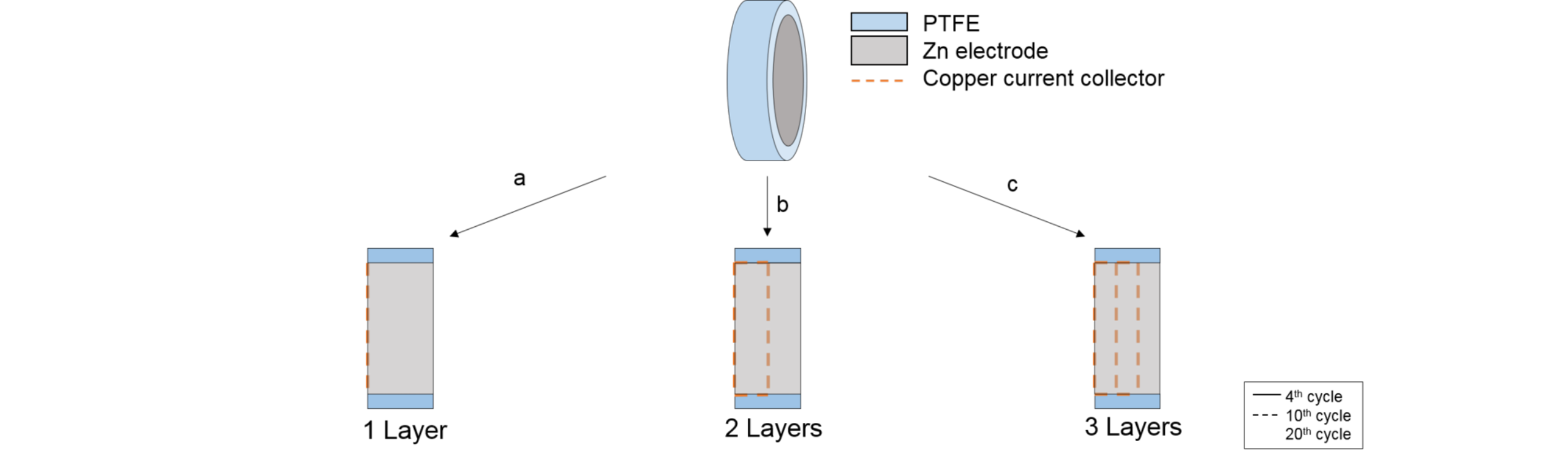
PTFE
Zn electrode
Copper current collector
a
b
c
1 Layer
2 Layers
3 Layers
4th cycle
10th cycle
20th cycle

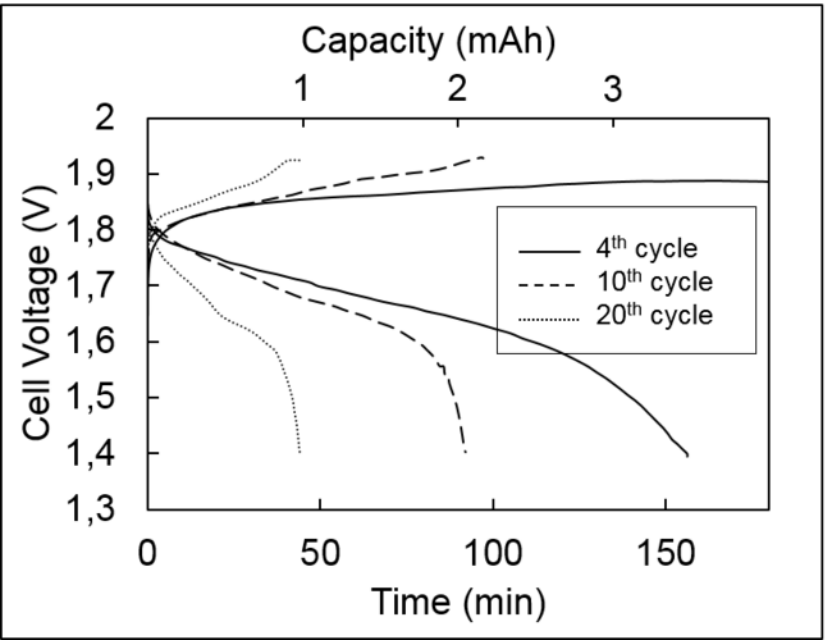
Capacity (mAh)
Cell Voltage (V)
Time (min)
4th cycle
10th cycle
20th cycle

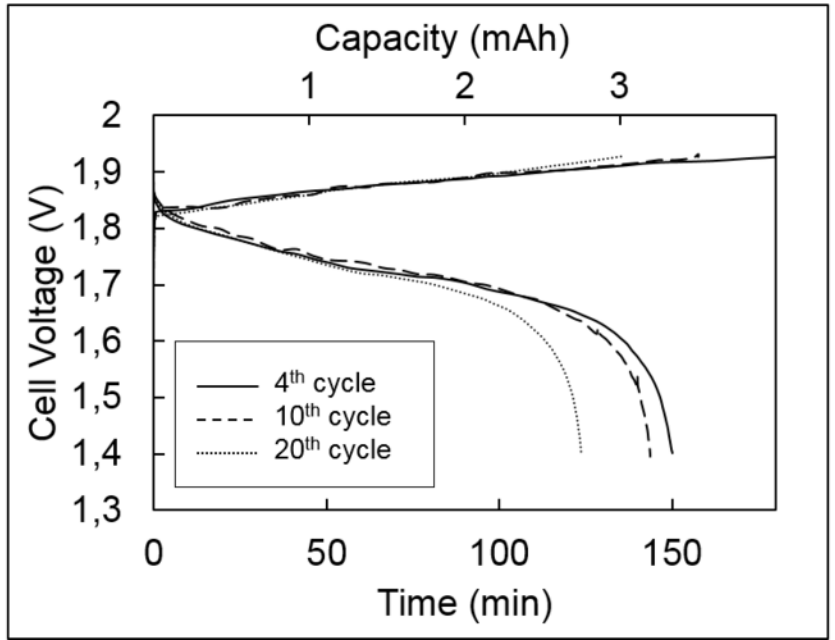
Capacity (mAh)
Cell Voltage (V)
Time (min)
4th cycle
10th cycle
20th cycle

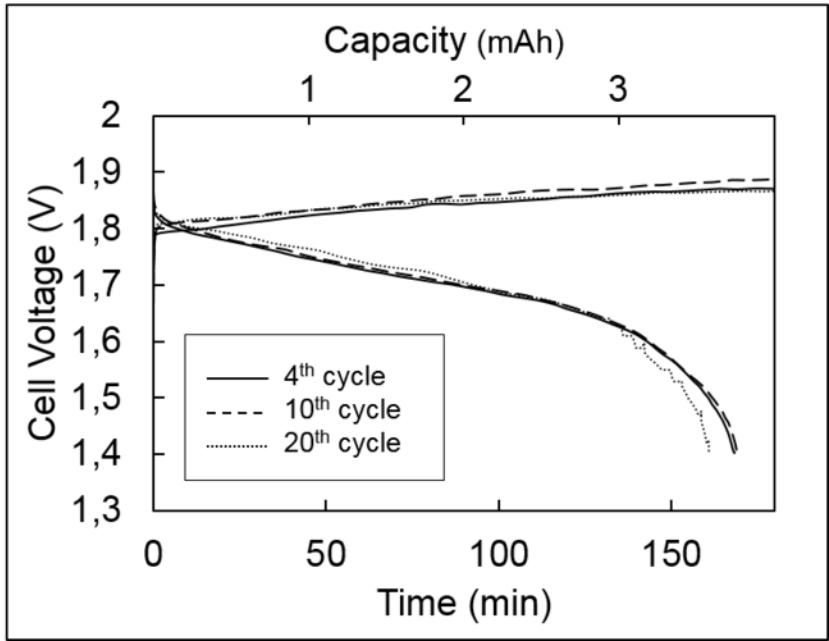
Capacity (mAh)
Cell Voltage (V)
Time (min)
4th cycle
10th cycle
20th cycle